Available online at www.sciencedirect.com
SCIENCE DIRECT®
International Journal of Mass Spectrometry 225 (2003) 135–153
International Journal of Mass Spectrometry
www.elsevier.com/locate/ijms

Useful yields of MCs_x^+ clusters: a cesium concentration-dependent study on the Cation Mass Spectrometer (CMS)

T. Wirtz[a,*], H.-N. Migeon[a], H. Scherrer[b]

[a] *Laboratoire d'Analyse des Matériaux, CRP—Gabriel Lippmann, 162A, av. de la Faïencerie, Luxembourg L-1511, Luxembourg*
[b] *Laboratoire de Physique des Matériaux, Ecole des Mines, Parc de Saurupt, F-54042 Nancy Cedex, France*

Received 2 April 2002; accepted 14 November 2002

Abstract

To optimize the advantageous quantification technique consisting in analyzing MCs_x^+ clusters, the Laboratoire d'Analyse des Matériaux (LAM) has developed a new instrument specially dedicated to performing this kind of analysis. The Cation Mass Spectrometer (CMS) instrument leads to high MCs_x^+ useful yields by allowing to reach an optimum value of the stationary Cs surface concentration, which is known to be a very critical parameter in MCs_x^+ analysis due to its strong influence on the probability of secondary Cs^+ ionization. The present work focuses on the potential of the CMS instrument to vary the stationary Cs concentration over a large range and the benefits concerning the MCs_x^+ useful yields resulting from this possibility. Analyses were performed on three different samples (Al, Si, Ni) while modifying the impact angle of the primary Cs^+ beam and in the Cs^+–Ga^+ cobombardment mode. These techniques are shown to be complementary with respect to the covered ranges of cesium concentrations resulting in a complete range going from quasi 0 to some 30%. The observed variations of the useful yields are discussed in terms of the stationary Cs concentration produced during the analysis and the consequent variations of the Cs^+ ionization probability provoked by work function shifts which were determined by in-situ measurements. A comparison between the performances of the CMS and those of classic Cameca instruments shows, depending on the element, useful yield enhancements up to a factor 90 mainly due to work function conditions resulting in high Cs^+ ionization probabilities.

Keywords: Secondary Ion Mass Spectrometry; Quantification; Cesium clusters; Useful yield; Cesium concentration; Ionization probability; Work function shifts

1. Introduction

Although Secondary Ion Mass Spectrometry (SIMS) is a very sensitive technique for surface and thin-film characterization because of its low detection limits and high dynamic range, it often suffers from serious quantification problems caused by the so called "matrix effect". This matrix effect, which stands for the strong dependence of the ionization probability of the secondary ions on the sample composition [1], can be circumvented by working in the MCs_x^+ mode. With this technique, the analyses are performed by bombarding the sample with Cs^+ ions and detecting MCs^+ clusters [2–6] and MCs_2^+ clusters [7,8] in the case of electronegative elements, M being the element to be analyzed. The quantitative potential of this

* Corresponding author. Tel.: +352-470261-511; fax: +352-470261-549.
E-mail address: wirtzt@crpgl.lu (T. Wirtz).

1387-3806/02/$ – see front matter
PII S1387-3806(02)01088-6

method is understood assuming that the MCs^+ ions are generated by the combination of a secondary neutral M^0 with a resputtered Cs^+ ion in the near surface region of the surface [3,5,9]. Consequently, the emission process for the species M is decoupled from the subsequent MCs^+ ion formation process in analogy to the ion formation in secondary neutral mass spectrometry resulting in a drastic decrease of the matrix effect.

It has been shown that the MCs^+ and $MCs_2{}^+$ yields strongly depend on the stationary cesium surface concentration incorporated in the specimen during the primary bombardment. An increasing Cs surface concentration can lower the electron work function below a critical value which is situated slightly below the ionization energy of Cs. If this occurs, according to the electron tunneling model for secondary ion formation, the probability of secondary Cs^+ ionization and consequently the probability of MCs^+ and $MCs_2{}^+$ cluster formation strongly decreases [4,10–14].

The analysis of $MCs_x{}^+$ clusters is currently performed using dynamic SIMS instruments equipped with a primary ion column delivering Cs^+ ions in order to incorporate Cs into the specimen. In this case, the primary bombardment conditions (mainly the impact energy and the incidence angle) as well as the characteristics of the investigated specimen imply a distinct total sputtering yield Y and consequently determine the cesium surface concentration c_{Cs} according to $c_{Cs} = 1/(1 + Y)$. It is however not likely that this, bombarding determined, Cs surface concentration is equal to the optimum concentration for highest $MCs_x{}^+$ yields.

The Cation Mass Spectrometer (CMS) instrument has been designed to optimize the analysis of these MCs^+ and $MCs_2{}^+$ clusters [15]. The CMS machine leads to high MCs^+ and $MCs_2{}^+$ useful yields by allowing to reach an optimum value of the mentioned stationary Cs surface concentration while keeping the high transmission tied to the use of a double focusing magnetic sector spectrometer.

In a recent work [16], we studied the behavior of $MCs_x{}^+$ cluster useful yields with respect to cesium concentration variations obtained by sputtering yield changes resulting from different impact angles of the primary Cs^+ beam. While this technique allowed to reach only cesium concentrations above a minimum value corresponding to the highest possible sputtering yield, this paper will focus on the potential of the CMS instrument to vary the stationary Cs surface concentration over a large range by using the already mentioned variations of the impact angle of the primary Cs^+ beam and by working in the Cs^+–Ga^+ cobombardment mode. These techniques are shown to be complementary regarding the covered ranges of cesium concentrations resulting in a complete range going from quasi 0 to some 30%. Analyses were performed on three different samples (Al, Si, Ni) which were mainly chosen for their work function values. The observed variations of the useful yields are discussed in terms of the stationary Cs concentration and of the resulting work function shifts which were determined by in-situ measurements.

2. Experimental

The design and the main characteristics of the CMS have already been published in previous works [15,16].

The desired changes of the stationary Cs surface concentration were obtained by applying two primary bombardment techniques. The first one consisted in bombarding the sample with a Cs^+ beam and using the z motion of the CMS sample stage in order to modify the distance d between the sample surface and the extraction nose and hence the impact angle θ, which is defined with respect to the surface normal, of the primary beam on the specimen [16]. Earlier measurements have shown that the transmission of the spectrometer is only weakly affected by changes of the distance d [15]. These variations of θ imply changes of the sputtering yield Y, which determines the Cs concentration. The CMS Cs^+ surface ionization gun was operated at a constant accelerating energy of 8.5 keV. Since the extraction voltage applied to the sample was 4500 V, the primary beam had an impact energy of 4 keV. As the distance d between the sample surface and the extraction nose varied for the present work between 1.7 and 2.9 mm, the cited energetic

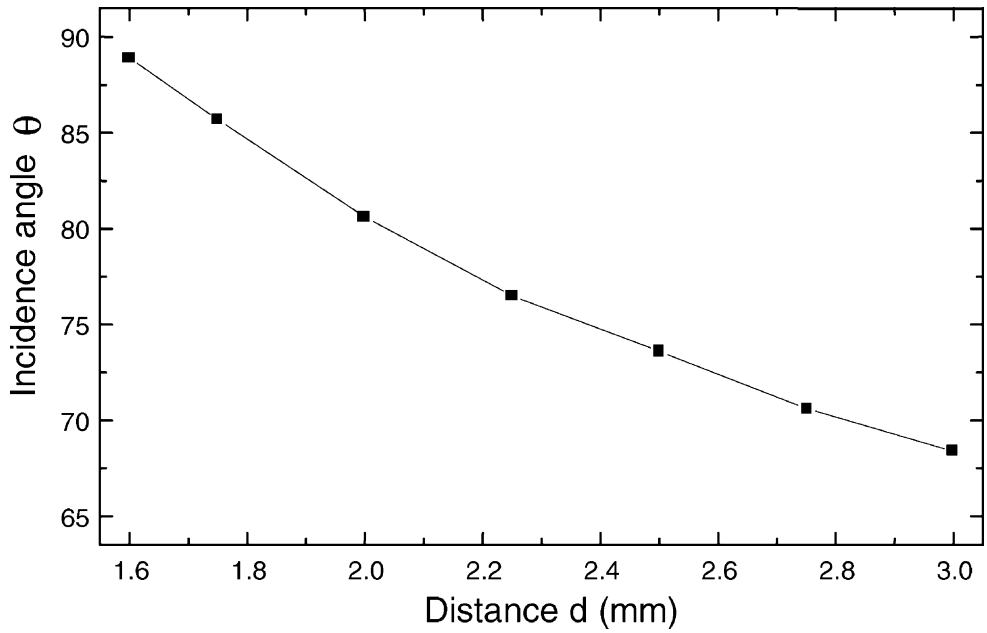

Fig. 1. Evolution of the incidence angle θ with the distance d between the sample surface and the extraction nose. The values of θ were calculated by means of SIMION ion optics simulations.

conditions allowed, as shown in Fig. 1, primary impact angles θ going from 69 to 86° (values calculated by SIMION ion optics simulations [17]). The primary beam was raster-scanned across a rectangular area varying from 230 μm × 220 μm to 480 μm × 220 μm with increasing incidence angle θ. Typical beam currents lay between 25 and 40 nA. For these series of measurements, secondary ions were accepted from a circular area on the sample surface limited to a diameter of 42 or 52 μm, defined by an aperture centered with respect to the scanning area. The mass spectrometer was operated at a mass resolution of $M/\Delta M = 300$ and with an energy bandpass $\Delta E = 130$ eV.

The second analysis technique consisted in running simultaneously the Cs^+ ion gun and the field emission Ga^+ source installed on the CMS [16]. While a first surface is raster-scanned with a Cs^+ beam, a second surface, which is concentric with the first one, is covered with a Ga^+ beam (Fig. 2). This operating mode allows to vary the Cs concentration by adjusting the Cs proportion of the primary bombardment in order to reach lower Cs concentrations compared to analyses performed with a pure Cs bombardment. The mentioned Cs proportion can be varied by adapting the bombardment densities of the Cs^+ and/or Ga^+ ions, respectively. For these measurements, the distance d was maintained constant at 2.5 mm and the sample potential was fixed at 4500 V. The Ga^+ gun was operated at an accelerating energy of 28 keV and delivered currents ranging from 2.8 to 4.0 nA at an impact angle of 54°. The Ga^+ beam was raster-scanned across an area lying between 70 μm × 70 μm and 190 μm × 190 μm. Concerning the Cs^+ gun, it was used at an accelerating energy of 8.5 keV resulting in an impact

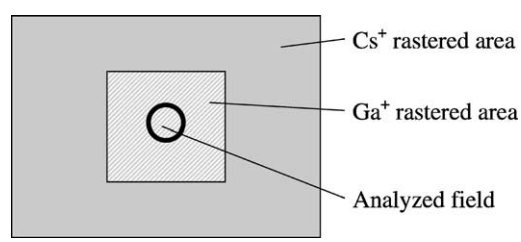

Fig. 2. Principles of the Cs^+–Ga^+ cobombardment technique.

angle of 74°. The Cs^+ currents lay between 15 and 30 nA. To obtain important variations of the Cs^+ bombardment density, the beam was raster-scanned over a large number of different areas ranging from 210 μm × 230 μm to 1800 μm × 2400 μm. For the measurements in the cobombardment mode, a field aperture was set to accept secondary ions from a circular area of 23 μm in diameter on the sample surface centered with respect to both the Cs^+ and Ga^+ scanning areas. The mass spectrometer was again operated at a mass resolution of $M/\Delta M = 300$ and with an energy bandpass $\Delta E = 130$ eV.

To measure the energy distributions of the secondary ions in both primary bombardment modes in order to determine work function shifts, the target potential was ramped around the 4500 V value while the remaining secondary beam optics were maintained unchanged. This ramping can be done on the CMS with a minimum step of 0.05 V providing a good accuracy of the measurements. The energy slit was closed to a bandpass $\Delta E = 2$–3 eV and secondary ions were accepted from a circular area of 42 μm in diameter.

For the present study, depth profiles and energy spectra were performed on Al, Si and Ni samples. These elemental samples were mainly chosen because of the different values of their work function: $\Phi_{Al} = 4.28$ eV, $\Phi_{Si} = 4.85$ eV, $\Phi_{Ni} = 5.15$ eV [18].

At the end of the analyses, the post-bombardment craters were measured with a Tencor P-10 profilometer.

3. Results and discussion

3.1. Accessible range of Cs concentrations

The variation of the incidence angle θ under a pure Cs^+ bombardment at a constant impact energy implies important sputtering yield changes. The Al sample leads to the highest sputtering yields among the three samples which were studied, with values ranging from 2.7 to 13.0. For the Ni sample, sputtering yields between 2.2 and 11.6 are reached. The Si sample shows the lowest sputtering yields, with values between 3.0 and 9.7. The sputtering yield curves for the three samples exhibit a quite flat summit which is situated between 2.4 and 2.8 mm. According to the SIMION ion optics simulations (Fig. 1), this distance range should correspond to incidence angles θ lying between 70 and 75°, which is consistent with experimental and theoretical results predicting a maximum of the sputtering yield occurring between 60 and 80° [19].

Considering simple retention models, the stationary Cs concentration c_{Cs} can be derived from the measured sputtering yield by applying [20,21]:

$$c_{Cs} = \frac{1}{1+Y} \quad (1)$$

One should however notice that the absolute value of c_{Cs} may differ from the value calculated with the first order approximation (1) at high Cs concentrations [22].

Fig. 3 shows the evolution of the Cs concentration with respect to the distance d for the three samples. As d decreases from 2.9 to 2.2 mm for any of the three samples, there are only little variations of c_{Cs}. This finding is due to the fact that these distances correspond to a range of incidence angles θ (69–77°) around the summit of the sputtering yield curve and imply thus only very little changes of the sputtering yield. Once d becomes lower than 2.2 mm, the increasing incidence angle (77–86°) allows to explore the steep decreasing section located on the right-hand side of the summit of the sputtering yield curve. As a consequence, the stationary Cs concentration in the sample rises.

The highest Cs concentrations that could be reached in the present study are situated between 25 and 30%. The minimum value of c_{Cs} under a pure Cs^+ bombardment is a consequence of the maximum value of the sputtering yield and depends thus on the sample. While Al leads to the lowest reachable minimum with 7.1%, the minimums for Ni and Si are 8.0 and 9.4%, respectively.

To gain access to lower Cs concentrations than the mentioned minimum values reached while modifying the incidence angle, further analyses were

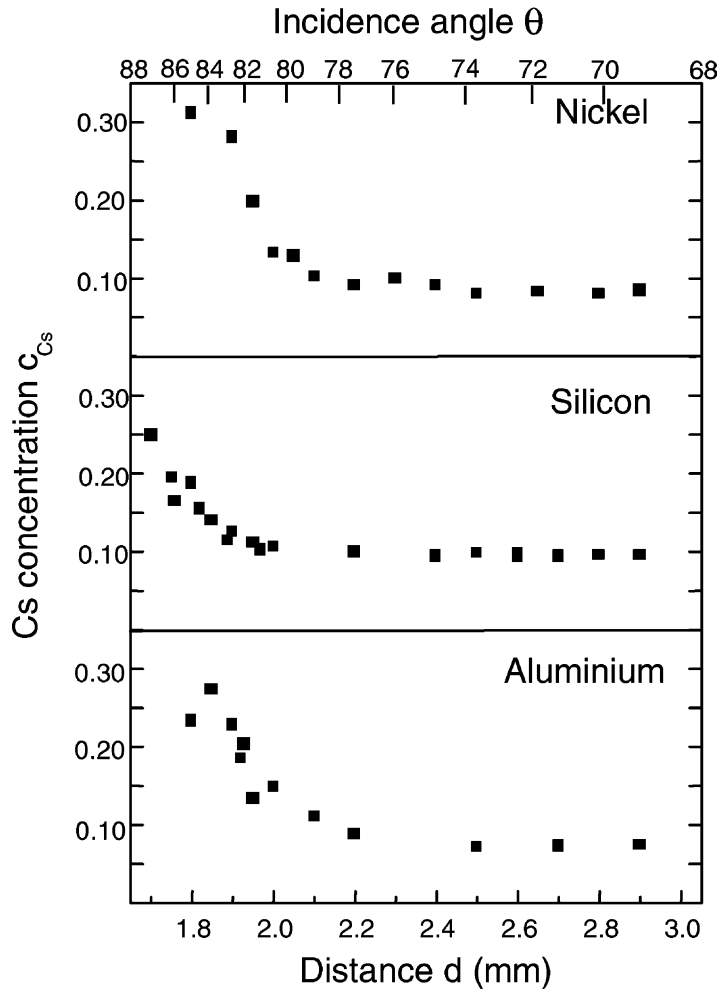

Fig. 3. Evolution of the Cs concentration with respect to the distance d between the sample surface and the extraction nose under a pure Cs^+ bombardment for the three investigated samples.

performed in the Cs^+–Ga^+ cobombardment mode. This technique consists in bombarding the sample simultaneously with Cs^+ and Ga^+ ions and adapting the proportion between both current densities in order to obtain lower Cs concentrations compared to those reached with a pure Cs^+ bombardment. To characterize the analysis conditions, we define a parameter η giving the proportion of Cs^+ ions contained in the primary bombardment:

$$\eta = \frac{j_{Cs}}{j_{Cs} + j_{Ga}} \quad (2)$$

j_{Cs} and j_{Ga} represent the Cs^+ and Ga^+ bombardment densities, respectively.

While $\eta = 0$ corresponds to a simple Ga^+ bombardment and thus to $c_{Cs} = 0$, $\eta = 1$ refers to a pure Cs^+ bombardment and will thus lead to the highest possible Cs concentration for the chosen analysis conditions, which are fixed in the present study by the incidence angle θ through the distance d. The distance d was therefore fixed at 2.5 mm, which, as was discussed earlier, was shown to be the center value of the distance range leading to the lowest Cs concentrations for a

given series of measurements. As a consequence, both primary bombardment techniques will be complementary, as the maximum Cs concentration reached with the Cs^+–Ga^+ cobombardment method corresponds to the minimum Cs concentration obtained while using a pure Cs^+ bombardment and varying the incidence angle of the primary beam on the sample.

After each analysis in the cobombardment mode, the stationary Cs concentration during the analysis was calculated using the following relation:

$$c_{Cs} = \frac{n_{Cs}}{n_M + n_{Cs} + n_{Ga}} \quad (3)$$

n_M represents the number of matrix atoms contained in the analyzed volume which was derived from the crater depth, the diameter of the analyzed field and the target density. n_{Cs} and n_{Ga} give the numbers of Cs and Ga atoms introduced into this same volume during the analysis and are calculated considering the bombardment densities of the respective ion beams, the diameter of the analyzed field and the bombardment time.

The evolution of the obtained Cs concentrations with respect to the parameter η for the three samples is represented in Fig. 4. These curves show that the cobombardment technique allows to vary the Cs concentration continuously from 0 to a maximum value which depends on the impact angle and energy of the Cs^+ beam and of course on the sample.

As a consequence, the two different analysis techniques which were used in the present work are

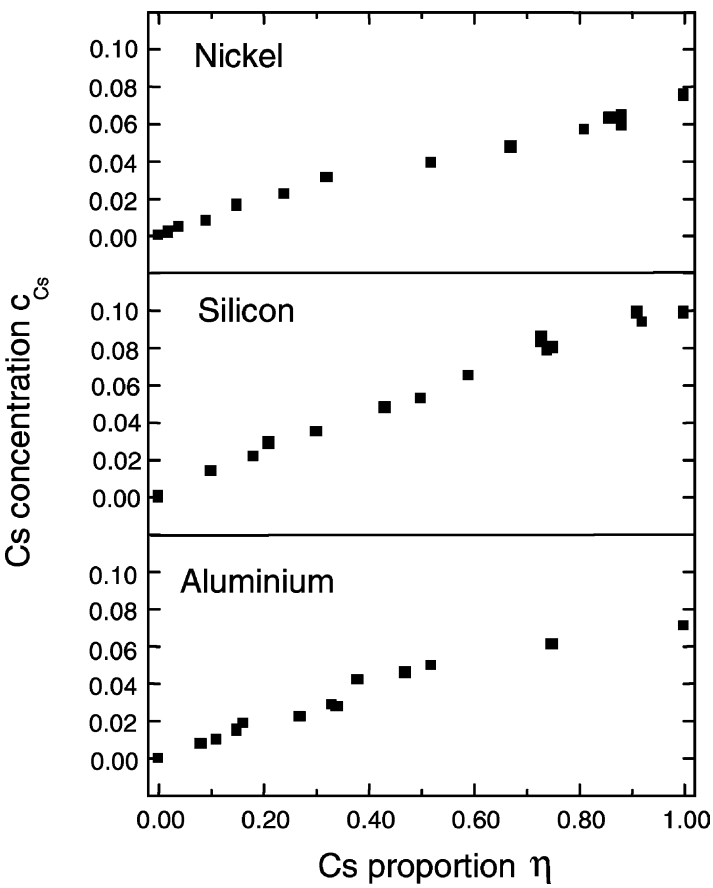

Fig. 4. Evolution of the Cs concentration with respect to the Cs proportion η obtained in the Cs^+–Ga^+ cobombardment mode for the three investigated samples.

complementary and allow to cover a continuous range of Cs concentrations going from 0 up to some 25–30%.

3.2. Influence of c_{Cs} on the MCs_x^+ signals

3.2.1. Results

The next step will now consist in studying the behavior of the measured secondary ions while varying the Cs concentration over the accessible range.

For a large number of different Cs concentrations, we performed depth profiles on the three studied samples while detecting the Cs^+, Cs_2^+, MCs^+ and MCs_2^+ signals, where M designates the matrix element. An exception nevertheless had to be made for the Ni sample, as the $NiCs_2^+$ cluster could not be detected because of its mass which exceeds the allowed maximum of 300.

The useful yield of an element M detected as a MCs_x^+ cluster is defined as follows:

$$\mathrm{UY}(MCs_x^+) = \frac{\text{number of detected } MCs_x^+ \text{ ions}}{\text{number of sputtered M atoms}} \quad (4)$$

On the other hand, the useful yield of the measured Cs_x^+ clusters is given by

$$\mathrm{UY}(Cs_x^+) = \frac{\text{number of detected } Cs_x^+ \text{ ions}}{\text{number of } Cs^+ \text{ ions incorporated into the analyzed volume}} \quad (5)$$

For each depth profile, the useful yields of the interesting species were calculated for the stationary regime as shown in formulas (4) and (5) and reported with respect to the corresponding Cs concentration in Fig. 5a–c for the respective samples.

Fig. 5a shows the existence of a critical Cs concentration of approximately 7% for the Al sample. This optimum concentration leads to maximum useful yields of 4.8×10^{-4} for $AlCs^+$, 1.8×10^{-5} for $AlCs_2^+$, and 6.1×10^{-3} for Cs_2^+. If c_{Cs} becomes lower or larger than the optimum value, the $AlCs^+$, $AlCs_2^+$ and Cs_2^+ useful yields decrease quickly. In the case of a Cs concentration exceeding its critical value to tend to the highest possible value that could be reached, a decrease of a factor 40 for $AlCs^+$ and of 3–4 orders of magnitude for $AlCs_2^+$ and Cs_2^+ can be noticed. On the other hand, the Cs^+ useful yield stays stable around a value of approximately 0.3 until the critical concentration of 7% is reached and drops by some 2 orders of magnitude at high concentrations.

A similar behavior can be noticed for the Si sample (Fig. 5b). The optimum concentration is found at about 10% and the maximum useful yields are 7.3×10^{-5} for $SiCs^+$, 1.0×10^{-5} for $SiCs_2^+$, and 2.6×10^{-3} for Cs_2^+. Again, an important decrease can be observed for the $SiCs^+$, $SiCs_2^+$ and Cs_2^+ useful yields if the Cs concentration becomes lower or higher than its critical value. Similarly to what was noticed for the Al sample, the Cs^+ useful yield determined for the Si sample stays stable around 0.3 until the critical concentration of 10% is reached and decreases by more than 2 orders of magnitude afterwards.

The Ni sample finally exhibits quite a different behavior (Fig. 5c). On the one hand, for Cs concentrations lower than the optimum value which is approximately 8%, one can still notice the same trend as for Al and Si, namely a decrease of the $NiCs^+$ and Cs_2^+ useful yields and a constant value around 0.3 for the Cs^+ useful yield. On the other hand, if the critical Cs concentration is exceeded, the drop of the useful yields is far less pronounced than in the case of Al and Si. As a matter of fact, the useful yields determined at a concentration of 31% are only a factor 2–3 lower than their maximum values in the case of Cs^+ and $NiCs^+$ and a factor 16 in the case of Cs_2^+. The maximum values of the useful yield were found to be 2.1×10^{-4} for $NiCs^+$ and 3.0×10^{-3} for Cs_2^+.

3.2.2. Discussion

To discuss the observed evolution of the useful yields with the Cs concentration in general and the differences in behavior between the studied samples in particular, some theoretical considerations regarding the formation processes of Cs_x^+ and MCs_x^+ clusters have to be made.

The intensity of secondary Cs^+ ions can be written as

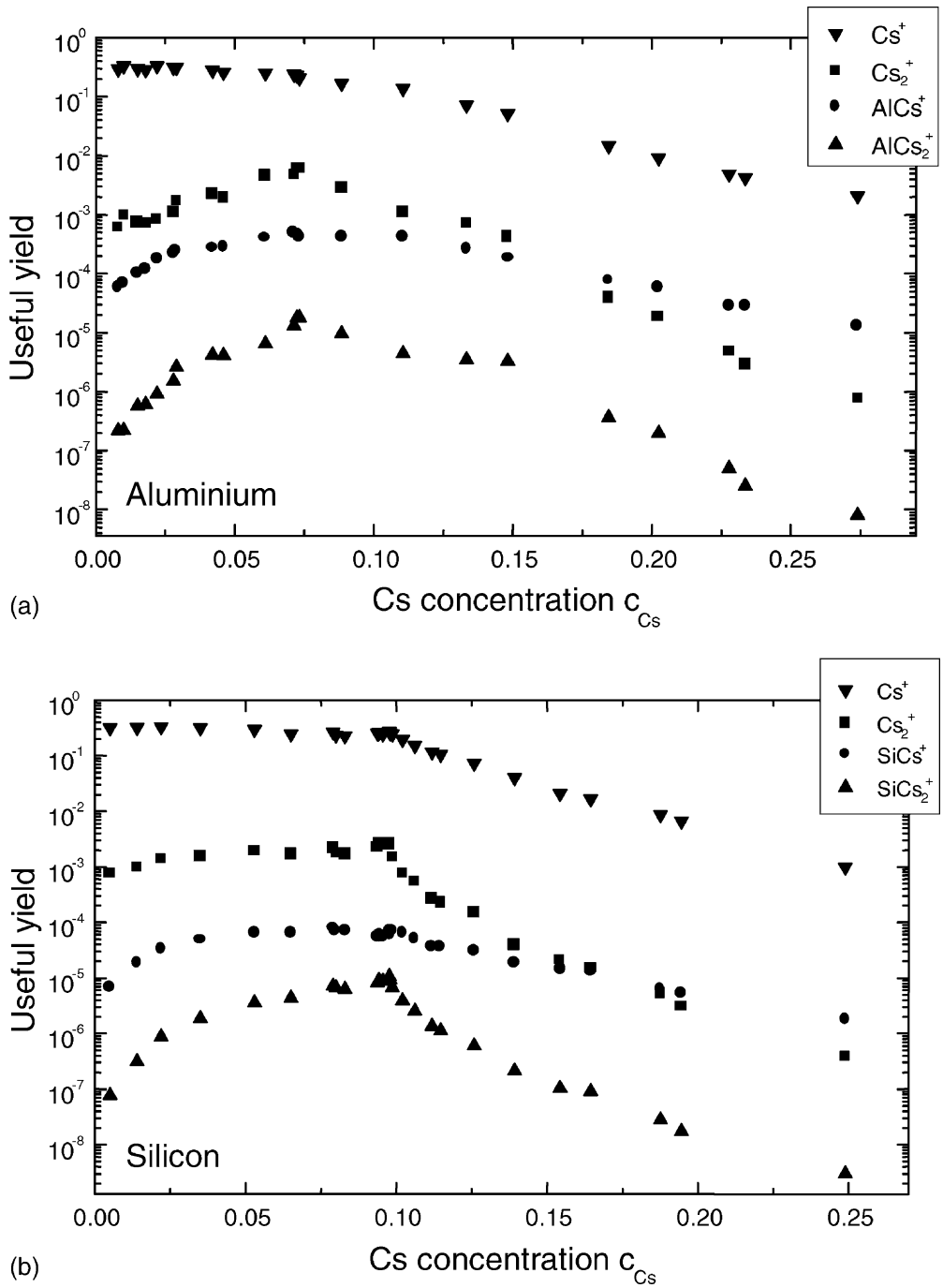

Fig. 5. (a) Useful yields determined for the Al sample as a function of the Cs concentration. (b) As (a), but for the Si sample. (c) As (a), but for the Ni sample.

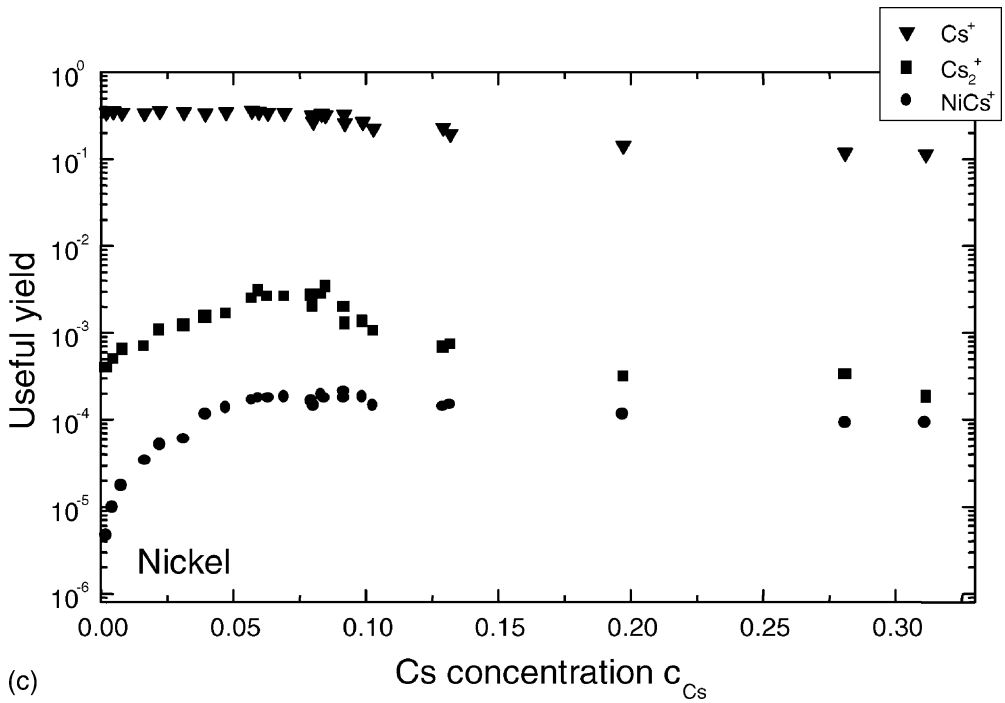

Fig. 5. (*Continued*).

$$I(\mathrm{Cs}^+) = I_\mathrm{p} \cdot Y \cdot c_\mathrm{Cs} \cdot \beta^+_\mathrm{Cs} \cdot \eta_{\mathrm{Cs}^+} \tag{6}$$

where I_p is the primary current, Y gives the sputtering yield, c_Cs is the stationary Cs concentration, β^+_Cs represents the ionization probability of a sputtered Cs atom, and η_{Cs^+} summarizes the transmission and detection efficiency of the Cs^+ ion.

On the other hand, $\mathrm{Cs_2}^+$ clusters are assumed to be formed via recombination of a neutral Cs and a Cs^+ ion in the near-surface region of the target [7,12,23]:

$$\mathrm{Cs}^0 + \mathrm{Cs}^+ \rightarrow \mathrm{Cs_2}^+ \tag{7}$$

The measured intensity of $\mathrm{Cs_2}^+$ clusters can therefore be expressed by

$$I(\mathrm{Cs_2}^+) = I_\mathrm{p} \cdot Y^2 \cdot (c_\mathrm{Cs})^2 \cdot \beta^+_\mathrm{Cs} \cdot (1 - \beta^+_\mathrm{Cs}) \cdot \gamma_{\mathrm{Cs}^0-\mathrm{Cs}^+} \cdot \eta_{\mathrm{Cs_2}^+} \tag{8}$$

$\gamma_{\mathrm{Cs}^0-\mathrm{Cs}^+}$ is a factor describing the recombination probability between, in this case, the independently sputtered Cs^0 and Cs^+.

MCs^+ clusters are formed by an atomic combination of a neutral M^0 and a Cs^+ ion sputtered in the same single event [3,5,9]:

$$\mathrm{M}^0 + \mathrm{Cs}^+ \rightarrow \mathrm{MCs}^+ \tag{9}$$

c_M being the concentration of the matrix element M, the measured intensity of MCs^+ clusters can therefore be expressed by

$$I(\mathrm{MCs}^+) = I_\mathrm{p} \cdot Y^2 \cdot c_\mathrm{M} \cdot c_\mathrm{Cs} \cdot \beta^+_\mathrm{Cs} \cdot \gamma_{\mathrm{M}^0-\mathrm{Cs}^+} \cdot \eta_{\mathrm{MCs}^+} \tag{10}$$

Concerning the $\mathrm{MCs_2}^+$ clusters, three different formation processes were proposed [7]:

$$\mathrm{M}^0 + \mathrm{Cs_2}^+ \rightarrow \mathrm{MCs_2}^+ \tag{11}$$

$$\mathrm{MCs}^0 + \mathrm{Cs}^+ \rightarrow \mathrm{MCs_2}^+ \tag{12}$$

$$\mathrm{M}^- + \mathrm{Cs}^+ + \mathrm{Cs}^+ \rightarrow \mathrm{MCs_2}^+ \tag{13}$$

While the first mechanism seems to be dominating in the case of an electropositive element M, the last two

become important for electronegative elements and thus increase their useful yield [7,12]. The MCs^0 occurring in the formation process (12) results from the neutralization of an MCs^+ ion by electronic capture [23].

The signals corresponding to the MCs_2^+ clusters originating from the three considered mechanisms can be written respectively [23,24]:

$$\text{for (11)}: \quad I(MCs_2^+) = I_p \cdot Y^3 \cdot c_M \cdot (c_{Cs})^2 \cdot \beta_{Cs}^+ \cdot (1-\beta_{Cs}^+) \cdot \gamma_{Cs^0-Cs^+} \cdot \gamma_{M^0-Cs_2^+} \cdot \eta_{MCs_2^+} \tag{14}$$

$$\text{for (12)}: \quad I(MCs_2^+) = I_p \cdot Y^3 \cdot c_M \cdot (c_{Cs})^2 \cdot (\beta_{Cs}^+)^2 \cdot \varepsilon \cdot \gamma_{M^0-Cs^+} \cdot \gamma_{MCs^0-Cs^+} \cdot \eta_{MCs_2^+} \tag{15}$$

$$\text{for (13)}: \quad I(MCs_2^+) = I_p \cdot Y^3 \cdot c_M \cdot (c_{Cs})^2 \cdot \beta_M^- \cdot (\beta_{Cs}^+)^2 \cdot \gamma_{M^- -Cs^+ -Cs^+} \cdot \eta_{MCs_2^+} \tag{16}$$

The factor ε appearing in relation (15) denotes the probability of a neutralization of a MCs^+ cluster by electronic capture.

The numbers of Cs and M atoms resputtered from the target during the analysis can be expressed as follows:

$$n(Cs) = \frac{I_p}{e_0} \cdot Y \cdot c_{Cs} \cdot t \tag{17}$$

$$n(M) = \frac{I_p}{e_0} \cdot Y \cdot c_M \cdot t \tag{18}$$

e_0 is the elementary charge and t denotes the total sputtering time.

Considering expressions (6) and (8) giving the Cs_x^+ intensities on the one hand and relation (17) concerning the number of sputtered Cs atoms on the other hand, the following relations for the useful yield can be deduced from (5):

$$UY(Cs^+) = \beta_{Cs}^+ \cdot \eta_{Cs^+} \tag{19}$$

$$UY(Cs_2^+) = Y \cdot c_{Cs} \cdot \beta_{Cs}^+ \cdot (1-\beta_{Cs}^+) \cdot \gamma_{Cs^0-Cs^+} \cdot \eta_{Cs_2^+} \tag{20}$$

In analogy, referring to expressions (10), (14)–(16) regarding the MCs_x^+ signals and relation (18) giving the number of sputtered M atoms, the MCs_x^+ useful yields defined by (4) can be written as

$$\text{for (9)}: \quad UY(MCs^+) = Y \cdot c_{Cs} \cdot \beta_{Cs}^+ \cdot \gamma_{M^0-Cs^+} \cdot \eta_{MCs^+} \tag{21}$$

$$\text{for (11)}: \quad UY(MCs_2^+) = Y^2 \cdot (c_{Cs})^2 \cdot \beta_{Cs}^+ \cdot (1-\beta_{Cs}^+) \cdot \gamma_{Cs^0-Cs^+} \cdot \gamma_{M^0-Cs_2^+} \cdot \eta_{MCs_2^+} \tag{22}$$

$$\text{for (12)}: \quad UY(MCs_2^+) = Y^2 \cdot (c_{Cs})^2 \cdot (\beta_{Cs}^+)^2 \cdot \varepsilon \cdot \gamma_{M^0-Cs^+} \cdot \gamma_{MCs^0-Cs^+} \cdot \eta_{MCs_2^+} \tag{23}$$

$$\text{for (13)}: \quad UY(MCs_2^+) = Y^2 \cdot (c_{Cs})^2 \cdot \beta_M^- \cdot (\beta_{Cs}^+)^2 \cdot \gamma_{M^- -Cs^+ -Cs^+} \cdot \eta_{MCs_2^+} \tag{24}$$

Relation (19) indicates that the useful yield of Cs^+ is directly proportional to the ionization probability of secondary Cs β_{Cs}^+. As a consequence, it can be concluded from Fig. 5a–c that β_{Cs}^+ stays constant until a critical value of the Cs concentration is reached. If one assumes that under these conditions the totality of sputtered Cs is ionized, i.e., $\beta_{Cs}^+ = 1$, the instrumental transmission factor of the CMS instrument can be determined to be between 30 and 35%. Furthermore, the observed drop of the Cs^+ useful yield happening at Cs concentrations higher than the critical value can be explained by a decrease of the ionization probability β_{Cs}^+.

The situation for Cs_2^+ and the MCs_x^+ clusters is more complex. In addition to their dependence on the ionization probability β_{Cs}^+, the Cs_2^+ and MCs^+ useful yields are proportional to the Cs concentration c_{Cs} ((20) and (21)) and the sputtering yield Y, while the MCs_2^+ useful yields vary like $(c_{Cs})^2 \cdot Y^2$

((22)–(24)). The decrease of the Cs_2^+ and MCs_x^+ useful yields at Cs concentrations lower than the critical value, which is a consequence of this proportionality to c_{Cs} or $(c_{Cs})^2$, can be interpreted as a lack of available Cs atoms to form the respective clusters. On the other hand, the decrease of the Cs_2^+ and MCs_x^+ useful yields at Cs concentrations above the critical value indicates that the rise of c_{Cs} is not sufficient to counterbalance the combined decrease of the ionization probability β_{Cs}^+ and of the sputtering yield Y.

The observed drop of the ionization probability β_{Cs}^+ should be due to a decrease of the work function below a critical value as a consequence of Cs incorporation. According to the electron tunneling model for secondary ion emission, β_{Cs}^+ should exhibit an exponential dependence on the work function Φ of the sample once Φ becomes lower than a critical value [10,11,25,26]:

$$\beta_{Cs}^+ \propto \begin{cases} 1, & \text{if } \Phi \geq I \\ \exp\left(-\dfrac{I-\Phi}{\varepsilon_0}\right), & \text{if } \Phi < I \end{cases} \quad (25)$$

I is the ionization potential of Cs and ε_0 is an experimental parameter considered to scale with the normal component of the secondary ion's emission velocity [11].

3.3. Determination of work function shifts

To check the validity of the explanation given above in the case of our experiments, we performed in-situ measurements of the work function shifts. To do so, energy spectra were recorded at various Cs concentrations using both primary bombardment techniques. As a matter of fact, shifts of the work function are detected as a variation of the contact potential between the sample and the electrostatic analyzer and they provoke in consequence shifts of the secondary ion energy spectra.

Preliminary experiments and earlier studies [27] showed that the work function shifts can be equally deduced from Cs^+ and MCs^+ energy spectra. In this study, we chose to record energy spectra of secondary Cs^+ ions. To determine with precision the work function shifts the spectra are normalized and displayed in a linear scale. The treated spectra obtained for each one of the three samples are represented in Fig. 6a–c for the pure Cs^+ bombardment with variations of the distance d and in Fig. 7a–c for the Cs^+–Ga^+ cobombardment mode with variations of the parameter η. These graphs show that the whole distributions are shifted with respect to the energy axis while their shape remains essentially unchanged. In order to measure these shifts most accurately, the steeply rising low energy parts of the distributions were fitted with tangents whose intercepts with the energy axis were taken as a marker of the spectrum's position [27–29].

The obtained work function shifts $\Delta\Phi$ for each of the three investigated samples are reported with respect to the Cs concentration c_{Cs} in Fig. 8. The energy value determined from the spectrum recorded in the Cs^+–Ga^+ cobombardment mode at $\eta = 0.01$ is set as origin of the work function scale, as it corresponds to the lowest Cs concentration reached during our experiments. In order to merge in a same plot the work function shifts obtained by both primary bombardment techniques, the value corresponding to $d = 2.5$ mm taken out of the pure Cs^+ bombardment series was superposed to the one referring to $\eta = 1$ coming from the Cs^+–Ga^+ cobombardment series as the two mentioned primary bombardment conditions and thus the Cs concentrations are strictly identical.

The maximum decreases of the work function determined for the three samples are quite different. As a matter of fact, while shifts of -2.5 eV at $c_{Cs} = 0.29$ and -2.2 eV at $c_{Cs} = 0.25$ were found for the Al and Si samples, respectively, the Ni sample exhibited a shift of only -1.3 eV at $c_{Cs} = 0.31$. The highest work function shift found here for Al is close to -2.44 eV which was determined as being the maximum work function shift which can be obtained on Al (1 1 1) during Cs adsorption [30]. It can be concluded from this comparison that, for the Al sample, a Cs concentration of approximately 30% allows to reach the minimum of the work function curve which was observed at a Cs coverage of 2.0×10^{14} atoms/cm^2 in [30]. Concerning Si, Cs adsorption experiments found a maximum work function shift of -3.4 eV at a coverage of 3.4×10^{14} atoms/cm^2 [31]. As a maximum shift

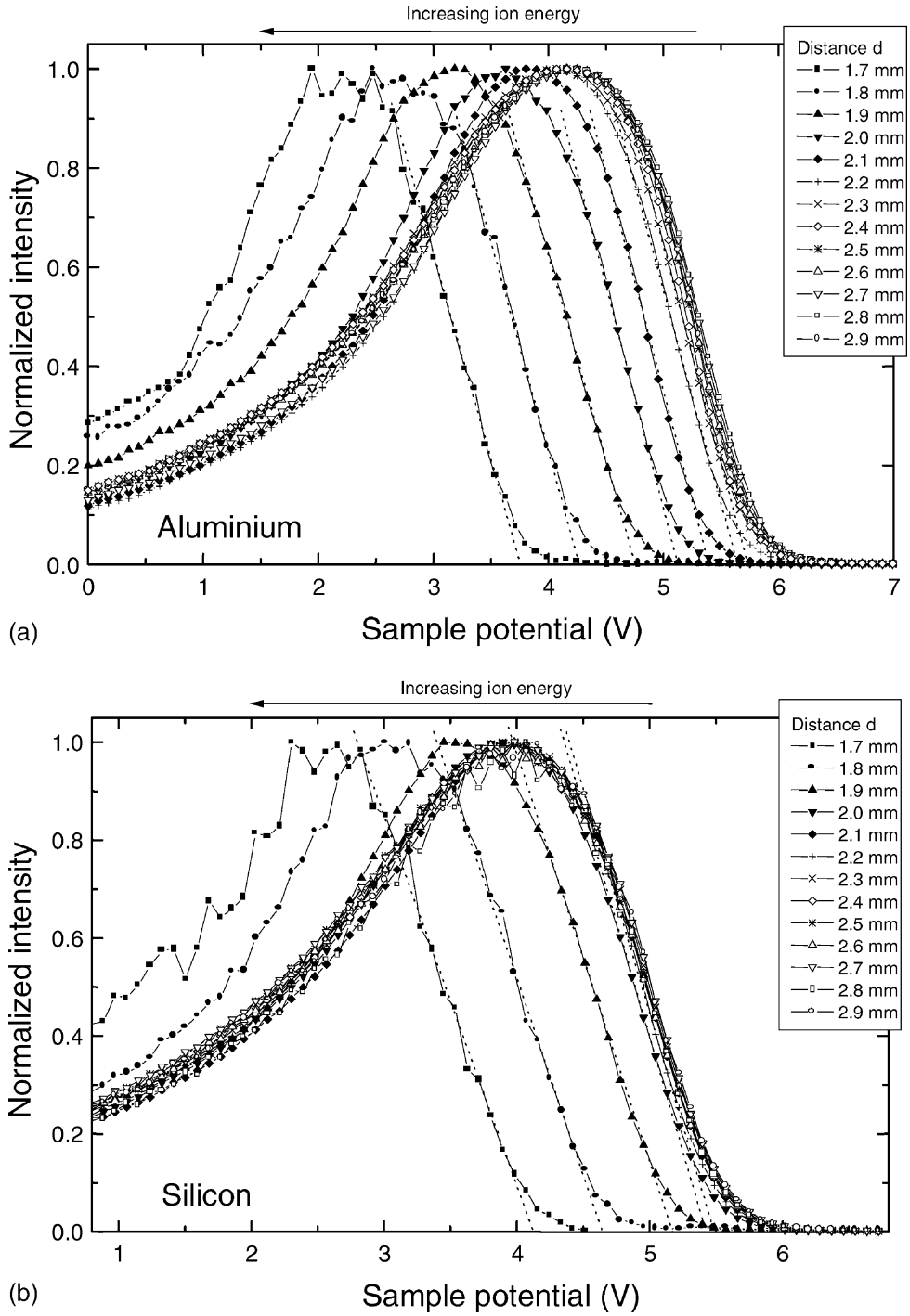

Fig. 6. (a) Normalized Cs^+ energy distributions obtained for the Al sample under a pure Cs^+ bombardment while changing the distance *d*. The sample potential is given relative to the nominal value of 4500 V. (b) As (a), but for the Si sample. (c) As (a), but for the Ni sample.

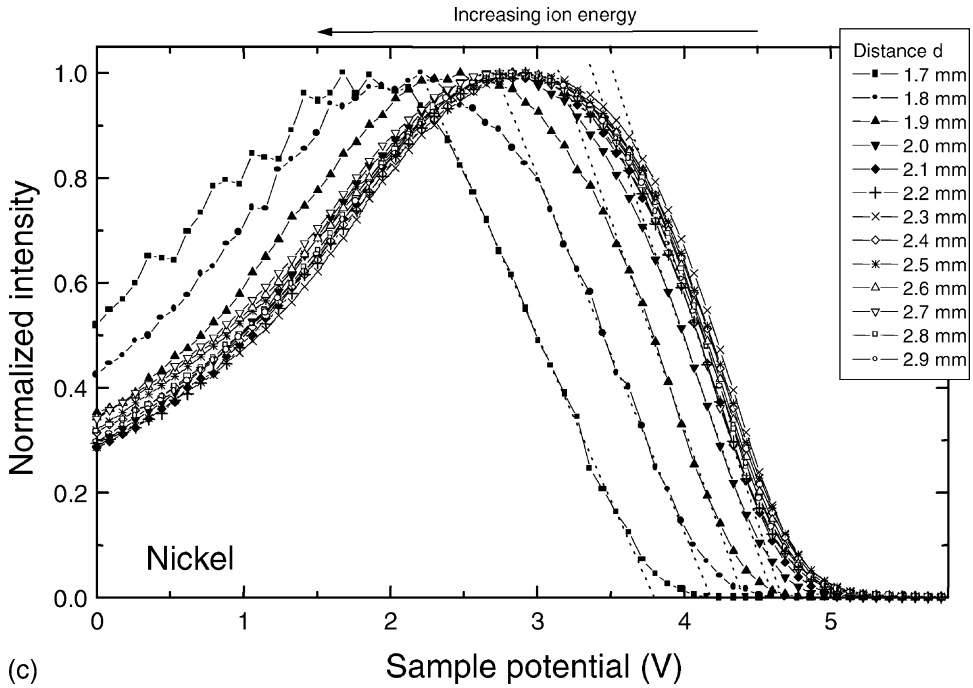

Fig. 6. (*Continued*).

of only −2.2 eV was observed for Si in the present work, the Cs concentrations obtained during the experiments on the Si sample were apparently not high enough to reach the minimum of the work function curve. For the nickel sample finally, a maximum work function shift of −3.1 eV was observed at a Cs coverage of 4.0×10^{14} atoms/cm^2 [32], which is twice the value needed for Al. This high necessary Cs coverage could explain the relatively weak shift of −1.3 eV found during the present study compared to the maximum value of −3.1 eV.

At this stage, it is interesting to plot the calculated ionization probabilities of secondary Cs β^+_{Cs} against the measured shifts of the work function. According to Eqs. (19) and (21), the behavior of β^+_{Cs} can most easily be traced by the useful yield of Cs^+ or by the useful yield of the MCs^+ clusters after a normalization with respect to the sputtering yield Y and the Cs concentration c_{Cs}. In consequence of these normalizations, the values of β^+_{Cs} deduced from the MCs^+ useful yields are affected by a higher uncertainty than those given directly by the Cs^+ useful yields. Nevertheless, Fig. 9a–c show that both β^+_{Cs} curves are running in an essentially parallel way, which confirms again the assumed MCs^+ formation mechanism (9).

The evolution of β^+_{Cs} with respect to the work function Φ shown for the three samples is typical for what one would expect considering relation (25) expressing the electron tunneling model. At work function values higher than a certain critical value, β^+_{Cs} stays essentially constant for each of the investigated samples. If Φ drops below this critical value, the ionization probabilities obtained for Al and Si exhibit an exponential decrease. For the Al sample the critical work function value can be determined as being 0.9 eV below the work function of pristine Al ($\Phi_{Al} = 4.28$ eV), which results in an absolute critical work function of approximately 3.4 eV. Concerning Si, the drop of β^+_{Cs} starts at about $\Delta\Phi = -0.9$ eV, which will lead to a value of 4.0 eV for the absolute critical work function. These data are in good agreement with [10], where the critical values were found at 3.4 eV too for an Al sample

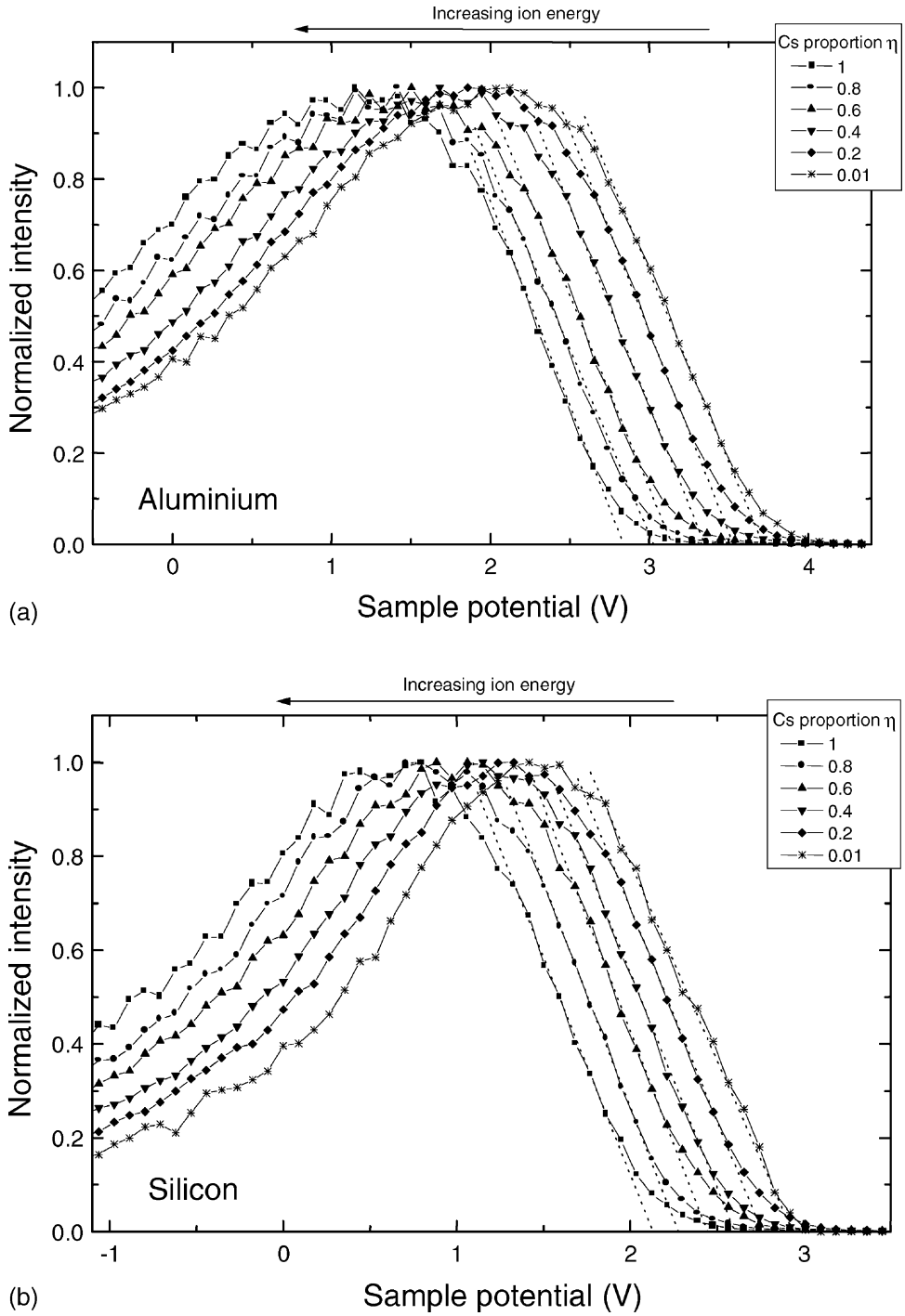

Fig. 7. (a) Normalized Cs^+ energy distributions obtained for the Al sample in the Cs^+–Ga^+ cobombardment mode while changing the parameter η. The sample potential is given relative to the nominal value of 4500 V. (b) As in (a), but for the Si sample. (c) As in (a), but for the Ni sample.

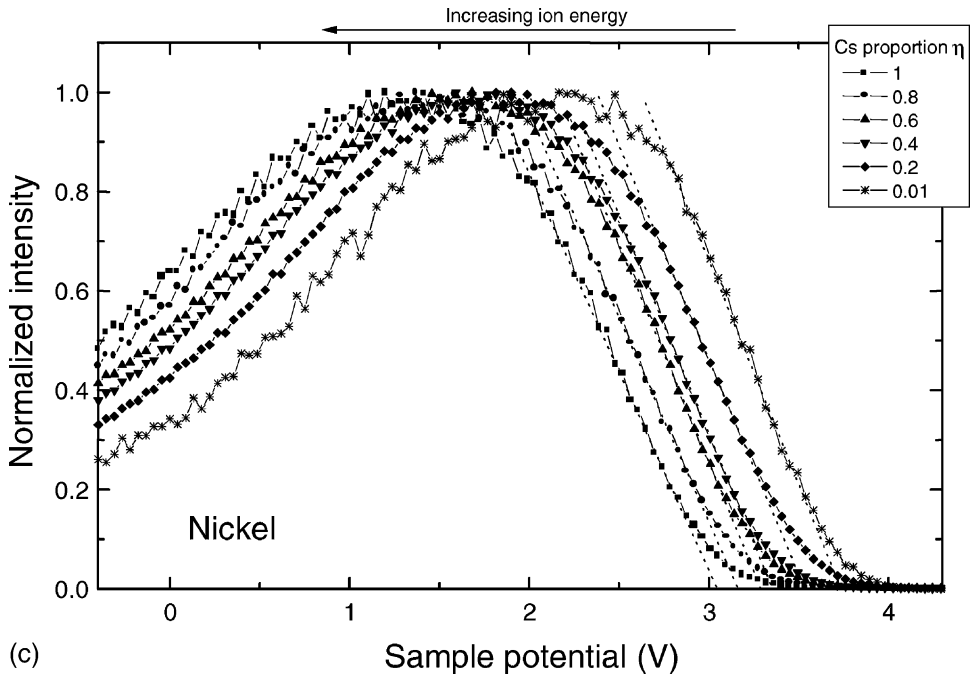

Fig. 7. (*Continued*).

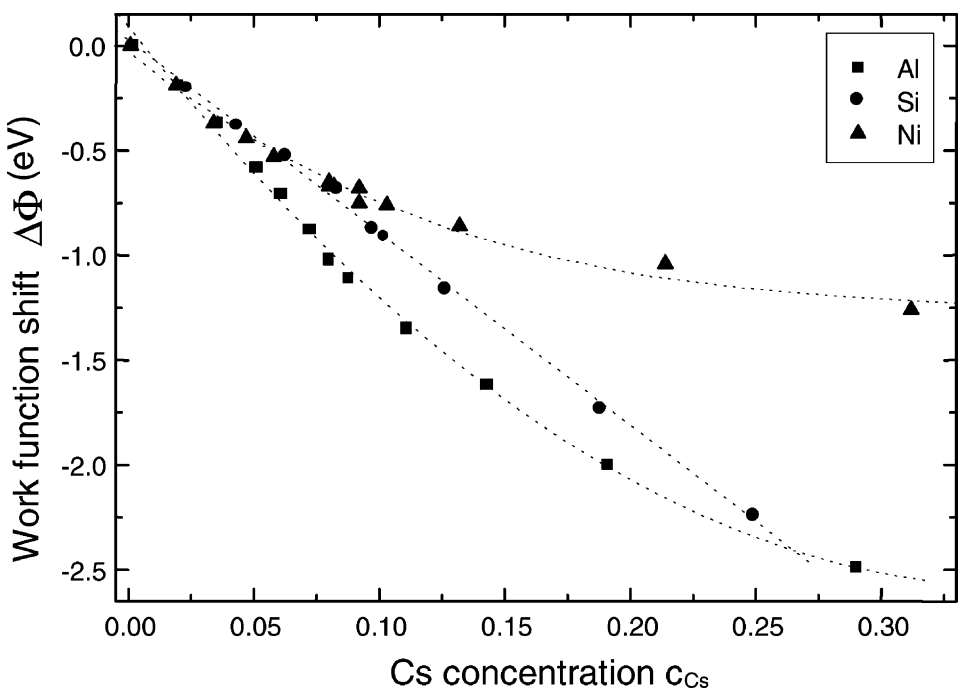

Fig. 8. Work function shifts determined from Figs. 6a–c and 7a–c with respect to the corresponding Cs concentration. The dotted curves are drawn only to guide the eye.

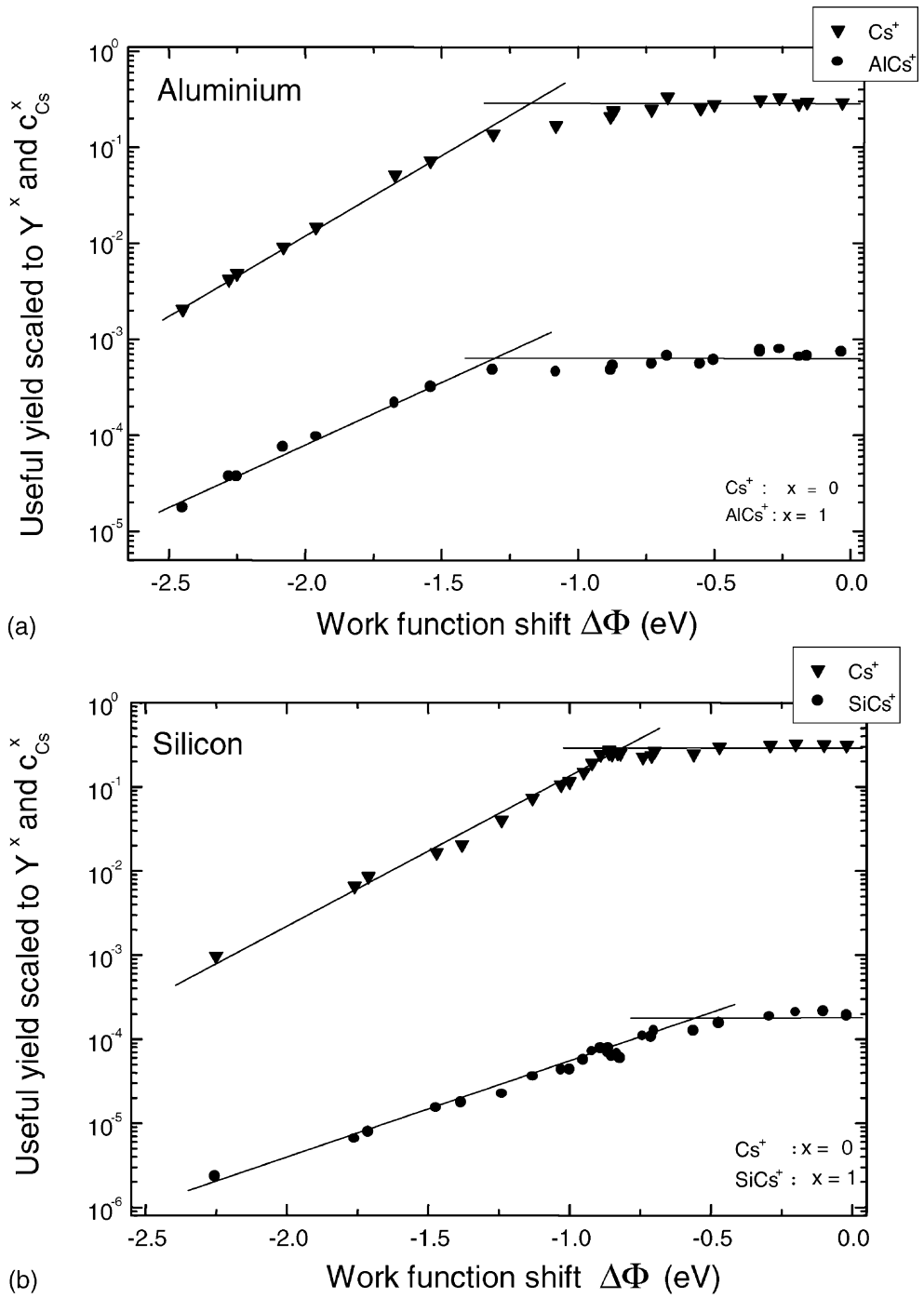

Fig. 9. (a) Evolution of the ionization probability β_{Cs}^{+} of secondary Cs deduced from the Cs^{+} useful yield and the normalized MCs^{+} useful yield vs. the measured work function shifts for the Al sample. (b) As in (a), but for the Si sample. (c) As in (a), but for the Ni sample.

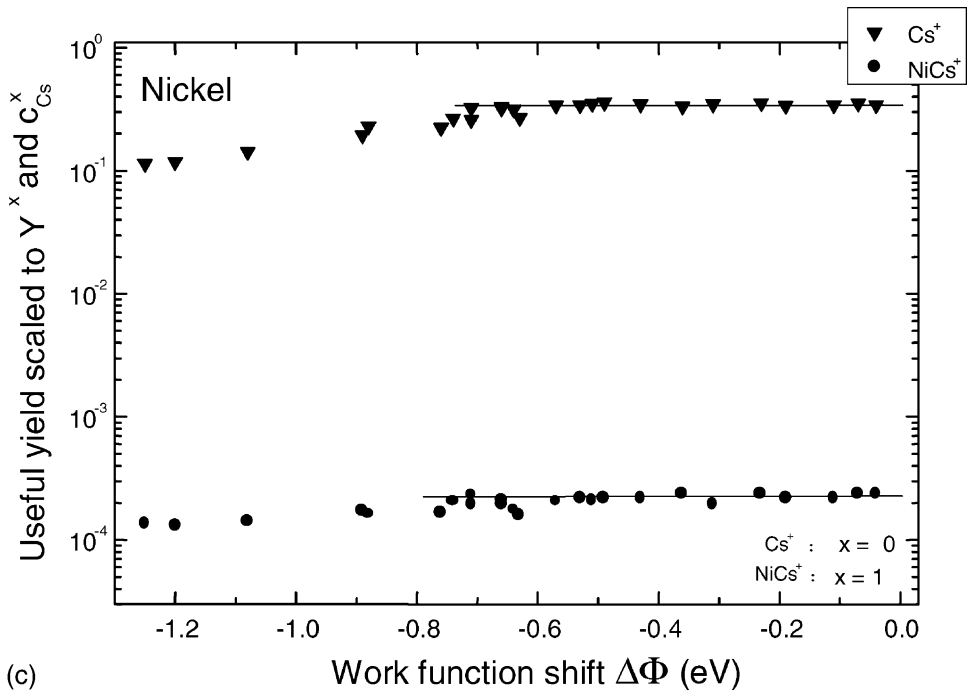

Fig. 9. (*Continued*).

and at some 3.7 eV for a Si sample, where the critical point is however far less distinct than for Al. For the Ni sample finally, no important drop of β^+_{Cs} can be observed. Assuming that the critical work function for Ni should be in the same range than the values found for Al and Si, the initial work function of the pristine Ni sample would have to be lowered by about 1.4–1.7 eV to reach the critical point. As the Cs concentrations accessible during our experiments did not provoke work function shifts at this extent for the Ni sample, the exponential decreasing part of the curve could not be reached.

3.4. Benefits

To show the benefits resulting from the possibility to vary the Cs concentration over a large range on the CMS instrument and thus to optimize this important parameter in MCs_x^+ cluster analysis, the same three samples were investigated on the Cameca IMS 4f [33] and on the Cameca IMS LAM [34]. Both instruments were operated under standard conditions, namely a sample potential of 4500 V and a primary accelerating energy of 10 keV leading to an incidence angle of the primary beam of 42°. The Cs^+ and MCs^+ useful yields obtained on the two Cameca instruments are practically identical and their mean values are reported together with the corresponding values resulting from the present study on the CMS in Table 1.

This comparison shows that the most important enhancement can be obtained for the Al sample with a ratio of 80–90. For Si, there is still an improvement of a factor 5–7, while the useful yields calculated for both types of instruments are absolutely identical for the Ni sample. These observations can be explained by the combination of several facts: Al has the lowest work function of the three investigated samples, its work function decreases quickly while increasing the Cs concentration and the ionization probability β^+_{Cs} determined from Al exhibits an immediate drop as soon as the work function falls below a critical value. The Cs concentration resulting from the standard

Table 1
Compilation of the maximum useful yields determined on the Cation Mass Spectrometer and on the Cameca IMS 4f and IMS LAM 6f instruments (mean value)

Sample	Signal	CMS	Cameca IMS 4f (Cameca IMS LAM 6f)	Ratio
Al ($\Phi = 4.28$ eV)	Cs^+	3.0×10^{-1}	3.8×10^{-3}	80
	$AlCs^+$	4.8×10^{-4}	5.4×10^{-6}	90
Si ($\Phi = 4.85$ eV)	Cs^+	3.0×10^{-1}	6.5×10^{-2}	5
	$SiCs^+$	7.3×10^{-5}	1.1×10^{-5}	7
Ni ($\Phi = 5.15$ eV)	Cs^+	3.2×10^{-1}	3.1×10^{-1}	1
	$NiCs^+$	2.1×10^{-4}	2.0×10^{-4}	1

Cameca conditions is thus too high for the Al sample and the corresponding β^+_{Cs} is far lower than the ideal value of 1. A similar explanation is valid for Si: the Cameca c_{Cs} value is already too high, but due to the higher work function of Si compared to Al, the drop of β^+_{Cs} is less important than it is for Al. Interestingly, measurements performed by Gnaser in dynamic Cs implantation conditions on a Si sample showed a decrease of the same factor 7 of β^+_{Cs} while c_{Cs} increased from 0 to the value dictated by the standard Cameca conditions [27]. Ni finally has the highest work function and it decreases in a lesser manner when the Cs concentration increases within the range which was accessible for the present study. As a consequence, the Cs concentration resulting from the Cameca conditions still allowed the highest possible ionization probability.

4. Conclusion

Analyses performed on three different samples (Al, Si, Ni) while modifying the impact angle of a pure Cs^+ primary beam and in the Cs^+–Ga^+ cobombardment mode have shown the possibility to vary the stationary Cs surface concentration on the Cation Mass Spectrometer. The two complementary primary bombardment techniques result in a continuous Cs concentration range going from quasi 0 to some 30%. This capability to adjust the Cs concentration allows the optimization of the measurement conditions in order to reach high MCs_x^+ useful yields. The observed decrease of the MCs_x^+ useful yields at Cs concentrations lower than the optimum value can be interpreted as a lack of available Cs atoms to form the clusters. The drop of the useful yields at Cs concentrations exceeding the critical value is shown to be a direct consequence of the strong decrease of the ionization probability of secondary Cs provoked by a lowering of the work function below a critical point. A comparison between the performances of the CMS and those of classic Cameca instruments shows that this possibility to adapt the Cs concentration to its optimum value leads to useful yield enhancements up to a factor 90.

References

[1] H.A. Storms, K.F. Brown, J.D. Stein, Anal. Chem. 49 (1977) 2023.
[2] Y. Gao, J. Appl. Phys. 64 (1988) 3760.
[3] H. Gnaser, H. Oechsner, Fresenius J. Anal. Chem. 341 (1991) 54.
[4] K. Wittmaack, Nucl. Instrum. Methods Phys. Res. B 64 (1992) 621.
[5] C.W. Magee, W.L. Harrington, E.M. Botnick, Int. J. Mass Spectrom. Ion Process. 103 (1990) 45.
[6] M.A. Ray, J.E. Baker, C.M. Loxton, J.E. Greene, J. Vac. Sci. Technol. A 6 (1) (1988) 44.
[7] Y. Gao, Y. Marie, F. Saldi, H.-N. Migeon, in: A. Benninghoven, Y. Nihei, R. Shimizu, H.W. Werner (Eds.), Secondary Ion Mass Spectrometry SIMS IX, Wiley, Chichester, 1994, p. 382.
[8] Y. Gao, Y. Marie, F. Saldi, H.-N. Migeon, in: A. Benninghoven, Y. Nihei, R. Shimizu, H.W. Werner (Eds.), Secondary Ion Mass Spectrometry SIMS IX, Wiley, Chichester, 1994, p. 406.
[9] T. Mootz, F. Adams, Int. J. Mass Spectrom. Ion Process. 152 (1996) 209.
[10] M.L. Yu, N.D. Lang, Phys. Rev. Lett. 50 (2) (1983) 127.
[11] M.L. Yu, Phys. Rev. B 29 (4) (1984) 2311.

[12] Y. Marie, Y. Gao, F. Saldi, H.-N. Migeon, Surf. Interface Anal. 23 (1995) 38.
[13] T. Kan, K. Mitsukawa, T. Ueyama, M. Takada, T. Yasue, T. Koshikawa, J. Surf. Anal. 5 (1999) 52.
[14] K. Wittmaack, Nucl. Instrum. Methods Phys. Res. B 85 (1994) 374.
[15] T. Mootz, B. Rasser, P. Sudraud, E. Niehuis, T. Wirtz, W. Bieck, H.-N. Migeon, in: A. Benninghoven, P. Bertrand, H.-N. Migeon, H.W. Werner (Eds.), Secondary Ion Mass Spectrometry SIMS XII, Elsevier, Amsterdam, 2000, p. 233.
[16] T. Wirtz, B. Duez, H.-N. Migeon, H. Scherrer, Int. J. Mass Spectrom. 209 (2001) 57.
[17] D.A. Dahl, SIMION 3D, Version 6.0.
[18] H.B. Michaelson, J. Appl. Phys. 48 (1977) 4729.
[19] H.H. Andersen, H.L. Bay, in: R. Behrisch (Ed.), Sputtering by Particle Bombardment I, Springer, Berlin, 1981, p. 145.
[20] F. Schulz, K. Wittmaack, Radiat. Eff. 29 (1976) 31.
[21] K. Wittmaack, in: A. Benninghoven, K.T.F. Janssen, J. Tümpner, H.W. Werner (Eds.), Secondary Ion Mass Spectrometry SIMS VIII, Wiley, Chichester, 1992, p. 91.
[22] J.E. Chelgren, W. Katz, V.R. Deline, C.A. Evans, R.J. Blattner, P. Williams, J. Vac. Sci. Technol. 16 (1979) 324.
[23] T. Mootz, A. Adriaens, F. Adams, Int. J. Mass Spectrom. Ion Process. 156 (1996) 1.
[24] Y. Marie, Doctoral Thesis, Institut National Polytechnique de Lorraine, 1995.
[25] J.K. Nørskov, B.I. Lundqvist, Phys. Rev. B 19 (11) (1979) 5661.
[26] N.D. Lang, Phys. Rev. B 27 (4) (1983) 2019.
[27] H. Gnaser, Phys. Rev. B 54 (23) (1996) 17141.
[28] M. Bernheim, F. Le Bourse, Nucl. Instrum. Methods Phys. Res. B 27 (1987) 94.
[29] M. Bernheim, G. Slodzian, in: A. Benninghoven, A.M. Huber, H.W. Werner (Eds.), Secondary Ion Mass Spectrometry SIMS VI, Wiley, Chichester, 1988, p. 139.
[30] A. Hohlfeld, M. Sunjic, K. Horn, J. Vac. Sci. Technol. A 5 (1987) 679.
[31] J.E. Ortega, E.M. Oellig, J. Ferron, R. Miranda, Phys. Rev. B 36 (1989) 6213.
[32] R.L. Gerlach, T.N. Rhodin, Surf. Sci. 19 (1970) 403.
[33] H.-N. Migeon, C. Le Pipec, J.J. Le Goux, in: A. Benninghoven, R.J. Colton, D.S. Simons, H.W. Werner (Eds.), Secondary Ion Mass Spectrometry SIMS V, Springer, Berlin, 1986, p. 155.
[34] W. Bieck, B. Rasser, M. Schuhmacher, P. Sudraud, H.-N. Migeon, in: A. Benninghoven, B. Hagenhoff, H.W. Werner (Eds.), Secondary Ion Mass Spectrometry SIMS X, Wiley, Chichester, 1997, p. 975.